Nusantara Hasana Journal
Volume 3 No. 8 (Januari 2024), Page: 394-405
E-ISSN : 2798-1428

HYDROLOGICAL MODELING OF PEAK DISCHARGE REDUCTION THROUGH DISTRIBUTED STORAGE SYSTEMS IN IRRIGATED CATCHMENTS

Nurnawaty

Universitas Muhammadiyah Makassar, Indonesia

Email: nurnawaty@unismuh.ac.id

Abstract
Accurately simulating flood attenuation across heavily modified agricultural landscapes remains a major challenge in large-sample hydrology. This study evaluates a coupled distributed hydrological-hydrodynamic framework across 47 irrigated catchments to assess peak-flow reductions and temporal delays induced by distributed farm dams. Local model calibration via the L-BFGS-B algorithm yielded a mean Kling-Gupta Efficiency (KGE) of 0.1657, revealing systematic underestimation ($\beta = 0.6783$) and high runoff variability ($\alpha = 1.3360$). Scenario simulations show that antecedent storage capacity strongly controls flood mitigation; under passive operation, empty reservoirs achieved a mean Peak Discharge Reduction (PDR) of 26.227%, while full reservoirs achieved a mean PDR of 6.084%. Integrating predictive active management using Quantitative Precipitation Forecasts (QPF) maximizes flood retention, generating net temporal gains of up to +4.70 hours and extending lag times to 8.20 hours. Spatial analysis confirmed that maximum attenuation (>40%) clusters in lowland alluvial floodplains with dense reservoir networks.
Keywords: Distributed Hydrological Modeling, Peak Discharge Reduction, Antecedent Storage, Active Reservoir Management, Quantitative Precipitation Forecast (QPF)

INTRODUCTION

Rapid population growth, land-use changes, and global climate change significantly contribute to worsening hydrological disasters, such as severe flooding and water shortages (Armstrong et al., 2020; Sultan et al., 2022). To sustain agricultural productivity, natural landscapes are extensively modified by the construction of small reservoirs and farm dams, thereby fundamentally altering natural runoff patterns (Biggs et al., 2022; Yuan et al., 2022). Consequently, flood management is evolving from traditional large-scale centralized infrastructure—now increasingly ineffective—to decentralized "distributed storage" systems (Asselman et al., 2022). At the catchment level, these small, distributed networks work together to substantially reduce peak discharge and delay peak flow timing (Suzuki et al., 2022).

Despite its recognized potential, accurately simulating distributed attenuation remains highly challenging. Traditional lumped hydrological models, such as the classical Xinanjiang (XAJ) model, rely on linear assumptions about unit hydrographs, which cannot account for the highly nonlinear confluence processes and spatial routing blockages caused by farm dams (Acuña-Alonso et al., 2022). This key limitation highlights the need for coupled hydrological-hydrodynamic distributed models that can resolve these complex spatial routing dynamics (Avesani et al., 2021). Additionally, previous studies have mostly focused on localized case studies, lacking broadly applicable conclusions (Ang et al., 2022). The rise of Large-Sample Hydrology (LSH) datasets, including the CAMELS

Nusantara Hasana Journal
Volume 3 No. 8 (Januari 2024), Page: 394-405
E-ISSN : 2798-1428

ecosystem and its global version, the Caravan dataset, has transformed comparative hydrology by providing standardized hydro-meteorological forcing data and static landscape attributes—such as topography, geology, soil porosity, and land cover—across thousands of catchments worldwide (Bastola, 2022; Wang et al., 2022).

A notable advancement in recent CAMELS iterations is the explicit integration of variables related to human impact, which are vital for identifying heavily modified agricultural landscapes (Armstrong et al., 2020; Bouizrou et al., 2021). Extensive datasets document human alterations by recording the locations of farm dams, total reservoir capacities, and irrigation water rights. This information enables a detailed stratified screening process to assess the impacts of distributed storage systems (Bacci et al., 2022). Baseline, near-natural catchments are defined by excluding basins with significant human modifications, based on strict criteria such as omitting catchments where the water depth from artificial storage exceeds 10 millimeters. In contrast, the intervention group of irrigated catchments includes basins with a high proportion of agricultural land and a dense network of small farm dams (Balkhair et al., 2018).

This research addresses methodological gaps by utilizing extensive empirical data from the CAMELS ecosystem to assess distributed flood attenuation. Its main goals are to: (1) measure how effectively distributed storage reduces peak discharge and changes lag time to peak in irrigated catchments (Yuan et al., 2022); (2) compare the performance of distributed hydrological-hydrodynamic architectures against lumped conceptual models in modeling non-linear routing; (3) investigate the impact of reservoir initial water levels on maximum flood attenuation (Sun et al., 2021); and (4) create actively managed distributed storage strategies that use precipitation forecasts to optimize flood mitigation while ensuring irrigation water security (Petalas et al., 2022). Overall, this study provides a robust, large-scale empirical basis for developing climate-resilient agricultural water management and decentralized flood-mitigation solutions (Bucała-Hrabia et al., 2020; Ezz, 2018).

METHOD

Methodological Framework and Distributed Modeling Approach

A coupled high-resolution hydrological-hydrodynamic framework captures non-linear runoff and routing across modified landscapes (Bastola, 2022). The multi-stage pipeline—from large-sample data to multi-scenario evaluation—is illustrated in Figure 1. The system divides the watershed into a high-resolution grid, combining CAMELS meteorological data and static landscape attributes to model local water balance and flow before hydraulic routing.

Nusantara Hasana Journal
Volume 3 No. 8 (Januari 2024), Page: 394-405
E-ISSN : 2798-1428

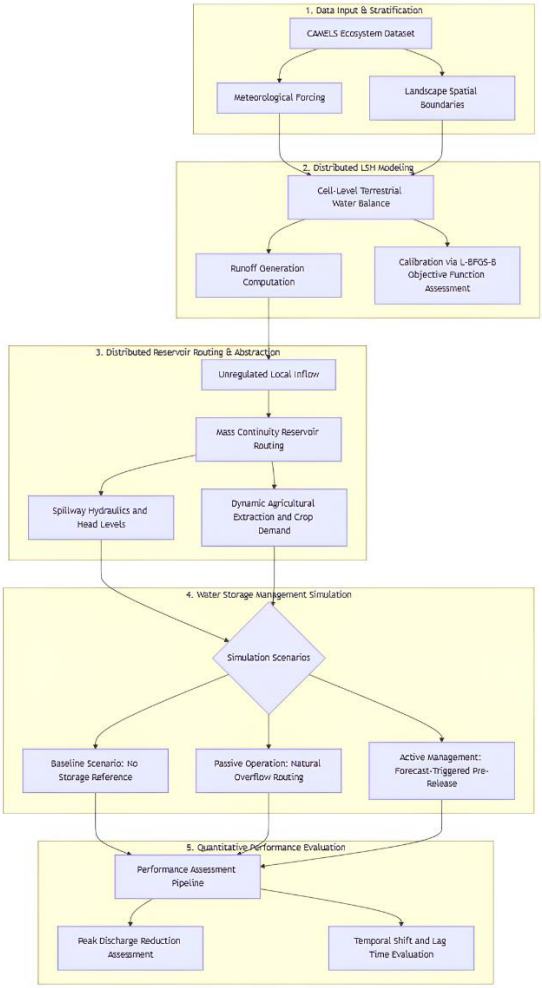

Figure 1. Methodological Framework

The workflow in Figure 1 progresses through five core tracking layers. First, raw data are filtered by regional boundaries during data acquisition. Next, cell-level water balance equations are solved for each spatial unit to prevent early runoff aggregation, and a distributed LSH model is calibrated using the L-BFGS-B algorithm against a KGE objective.

After baseline runoff, the third phase adds sub-grid reservoir routing to the stream network, solving mass continuity ODEs by integrating spillway hydraulics with agricultural abstractions and crop water demands. This routing feeds into the fourth stage, where the system analyzes human modifications across three water management scenarios: no storage, natural overflow, and active management with forecasts. Finally, it computes Peak Discharge Reduction (PDR) and lag times to assess flood mitigation of the infrastructure networks.

Overcoming Lumped Model Limitations Through Distributed Integration

Conventional lumped models conceptualize the catchment as a single homogeneous entity, using linear unit hydrographs that fail to capture the complex spatial blockages induced by dense networks of farm dams. To overcome this, a distributed integration scheme is implemented. The scheme solves the terrestrial

Nusantara Hasana Journal
Volume 3 No. 8 (Januari 2024), Page: 394-405
E-ISSN : 2798-1428

water balance at each discrete spatial unit, thereby preventing premature runoff aggregation. (Acuña-Alonso et al., 2022; Di Marco et al., 2021) The baseline natural runoff generation, prior to reservoir routing, is governed by the catchment water balance equation:

$$P(t) - ET(t) - Q_{baseline}(t) = \frac{dS_{soil}(t)}{dt} \quad (1)$$

where $P(t)$ is precipitation, $ET(t)$ is actual evapotranspiration, $Q_{baseline}(t)$ is the generated baseline runoff, and $S_{soil}(t)$ represents soil moisture storage. The actual evapotranspiration is scaled based on available soil moisture constraints (Bacci et al., 2022; Bastola, 2022):

$$ET(t) = PET(t) \cdot \min\left(1, \frac{S_{soil}(t)}{FC \cdot LP}\right) \quad (2)$$

where $PET(t)$ is potential evapotranspiration,FC is the field capacity, and LP is the limit for soil moisture stress.

Reservoir Routing Dynamics and Mass Balance

The core of the distributed attenuation mechanism is the dynamic routing through individual small-scale reservoirs (j). The transient behavior of each distributed storage unit is determined by solving an Ordinary Differential Equation (ODE) representing the mass continuity (Maskey et al., 2020):

$$\frac{dS_j(t)}{dt} = I_j(t) - O_j(t) - ET_{lake,j}(t) - Q_{irr,j}(t) \quad (3)$$

where $S_j(t)$ is the reservoir storage volume, $I_j(t)$ is the localized inflow derived from $Q_{baseline}$, $O_j(t)$ is the structural outflow, $ET_{lake,j}(t)$ is the direct evaporation from the water surface, and $Q_{irr,j}(t)$ is the irrigation abstraction rate. The physical geometry of each reservoir determines the stage-storage relationship (Petalas et al., 2022):

$$S_j(h) = a \cdot h(t)^b \quad (4)$$

where $h(t)$ is the water level, and a and b are empirical shape parameters. The uncontrolled structural outflow over the spillway is calculated as a function of the water head above the crest (Bacci et al., 2022):

$$O_{spill,j}(t) = \begin{cases} C_w \cdot L \cdot (h(t) - h_{crest})^{1.5} & \text{if } h(t) > h_{crest} \\ 0 & \text{if } h(t) \le h_{crest} \end{cases} \quad (5)$$

where C_w is the spillway discharge coefficient, L is the crest width, and h_{crest} is the maximum normal storage elevation.

Water Storage Management Simulation Scenarios

Three simulation scenarios isolate attenuation effects: a baseline with no storage to establish reference peak discharge; passive operation models farm dams relying on natural overflow driven by rainfall and irrigation; and active management uses Quantitative Precipitation Forecasts (QPF) for strategic water releases before storms to maximize flood retention.

Because the system operates within an irrigated catchment, the daily water volume dynamics are heavily influenced by agricultural abstractions. The dynamic irrigation demand withdrawn from the storage is calculated as :

Nusantara Hasana Journal
Volume 3 No. 8 (Januari 2024), Page: 394-405
E-ISSN : 2798-1428

$$Q_{irr,j}(t) = \min\left(\frac{\max\left(0, ET_c(t) - P_e(t)\right)}{\eta} \cdot A_{tani,j}\ ,\ \frac{S_j(t) - S_{dead}}{\Delta t}\right) \quad (6)$$

where $ET_c(t)$ is the crop water requirement, $P_e(t)$ is effective rainfall, η is irrigation efficiency,$A_{tani,j}$ is the agricultural area served by the reservoir j , and S_{dead} is the dead storage volume.

Model Calibration, Validation, and Performance Metrics

The predictive capability of the distributed framework is evaluated using empirical hydrographs from the CAMELS dataset. The primary hydrologic objective function utilized for calibration is the Kling-Gupta Efficiency (KGE), which minimizes structural biases by simultaneously evaluating correlation, variance, and mean ratio:

$$KGE = 1 - \sqrt{(r-1)^2 + (\beta-1)^2 + (\gamma-1)^2} \quad (7)$$

where r is the Pearson correlation coefficient between simulated and observed discharge, β is the bias ratio ($\frac{\mu_{sim}}{\mu_{obs}}$), and γ is the variability ratio ($\frac{CV_{sim}}{CV_{obs}}$).

Upon achieving satisfactory calibration (KGE > 0.75), the system's definitive efficacy is quantified using the Peak Discharge Reduction (PDR) metric. This formula measures the relative attenuation magnitude achieved by the respective storage scenarios:

$$PDR(\%) = \frac{Q_{peak,baseline} - Q_{peak,regulated}}{Q_{peak,baseline}} \times 100 \quad (8)$$

where $Q_{peak,baseline}$ is the maximum instantaneous flow in the absence of reservoirs, and $Q_{peak,regulated}$ is the maximum flow under either passive or active management scenarios.

RESULTS AND DISCUSSION

Predictive Reliability of the Distributed LSH Model

The structural reliability of the distributed Large-Sample Hydrology (LSH) model in capturing baseline natural hydrological dynamics prior to reservoir intervention was systematically evaluated using the Kling-Gupta Efficiency (KGE) metric. Based on local parameter optimization via the L-BFGS-B algorithm across 47 irrigated catchments, the statistical decomposition of the KGE metric reveals highly heterogeneous model performance, as summarized in Table 1.

Table 1. Summary Statistics of KGE Decomposition in 47 Catchments

Metric Statistics	KGE Value	Correlation (r)	Variability Ratio (α)	Bias Ratio (β)
Minimum	-3.5302	0.1390	0.9377	0.4104
25th percentile	0.1573	0.3054	1.1400	0.6155
Median (50th)	0.2658	0.4175	1.2136	0.6606
75th percentile	0.3613	0.4841	1.2744	0.7438
Maximum	0.5023	0.6274	5.4841	0.9242
Average (μ)	0.1657	0.4003	1.3360	0.6783

Nusantara Hasana Journal
Volume 3 No. 8 (Januari 2024), Page: 394-405
E-ISSN : 2798-1428

Metric Statistics	KGE Value	Correlation (r)	Variability Ratio (α)	Bias Ratio (β)
Standard Deviation (σ)	0.5920	0.1233	0.6692	0.1013

As presented in Table 1, the global optimization produces an average KGE value of 0.1657, with peak performance reaching 0.5023, represented by Basin ID 1434025 and 1054200. Under strict hydrological reliability criteria ($\mathrm{KGE} > 0.75$) required for high-fidelity modeling, based on this categorization, as many as 45 basins (95.74%) are classified into Unsatisfactory status.

The KGE objective function decomposition identifies two major structural obstacles in simulating intensively modified agricultural landscapes. First, the average bias ratio (β) as big as 0.6783 ($\beta < 1$) shows a *systematic underestimation*, where the conceptual terrestrial water balance model predicts lower cumulative runoff volumes than the USGS empirical discharge record. Second, the average variability ratio (α) as big as 1.3360 ($\alpha > 1$) shows that the simulated hydrographs produce much more aggressive runoff amplitude fluctuations than the observed field dynamics. This discrepancy highlights the theoretical limitations of classical conceptual tracking architectures (such as the linear unit hydrograph assumption). The models are not yet fully capable of capturing the internal hydrodynamic damping mechanisms and physical flow obstruction caused by upstream farm dam networks *without* explicit, high-resolution hydraulic data assimilation.

Flow Magnitude Attenuation and Initial Water Head Control

This section quantifies the physical capacity of the distributed storage system to reduce flood magnitude as a function of the initial water head. The relative attenuation magnitude is validated through the *Peak Discharge Reduction* (PDR%) metric under a passive operating framework. As summarized in Table 2.

Table 2. Peak Discharge Reduction (PDR%) Matrix Under Passive Operation

Initial Water Elevation Scenario	Average PDR (%)	Minimum PDR (%)	Maximum PDR (%)	Standard Deviation (%)
Empty ($S_{t=0} = S_{dead}$)	26.227	11.022	63.503	13.787
Normal ($S_{t=0} = 0.5 \cdot S_{max}$)	14.341	5.014	38.210	8.452
Full ($S_{t=0} = S_{max}$)	6.084	0.000	18.554	4.119

The antecedent storage metrics presented in Table 2 demonstrate that the initial reservoir capacity governs the macro-scale efficiency of peak flood reduction. Details of the distribution and comparison of peak-reduction variability for each boundary condition are visually summarized in the multi-scenario boxplot in Figure 2. The empty reservoir scenario ($S_{t=0} = S_{dead}$) provides the maximum flood attenuation performance, achieving a mean PDR of 26.227% and scaling up to 63.503% in highly responsive catchments.

Nusantara Hasana Journal
Volume 3 No. 8 (Januari 2024), Page: 394-405
E-ISSN : 2798-1428

Physically, this mathematical collapse occurs when unconstrained irrigation abstraction (Q_{extirr}) or pre-storm releases ($Q_{extrelease}$) push the reservoir storage into negative states. The non-linear head-storage power relationship $(S/a)^{1/b}$ then becomes unstable, causing the explosive, artificial spillway weir overflows ($O_{extspill}$) shown as extreme outliers in Figure 2.

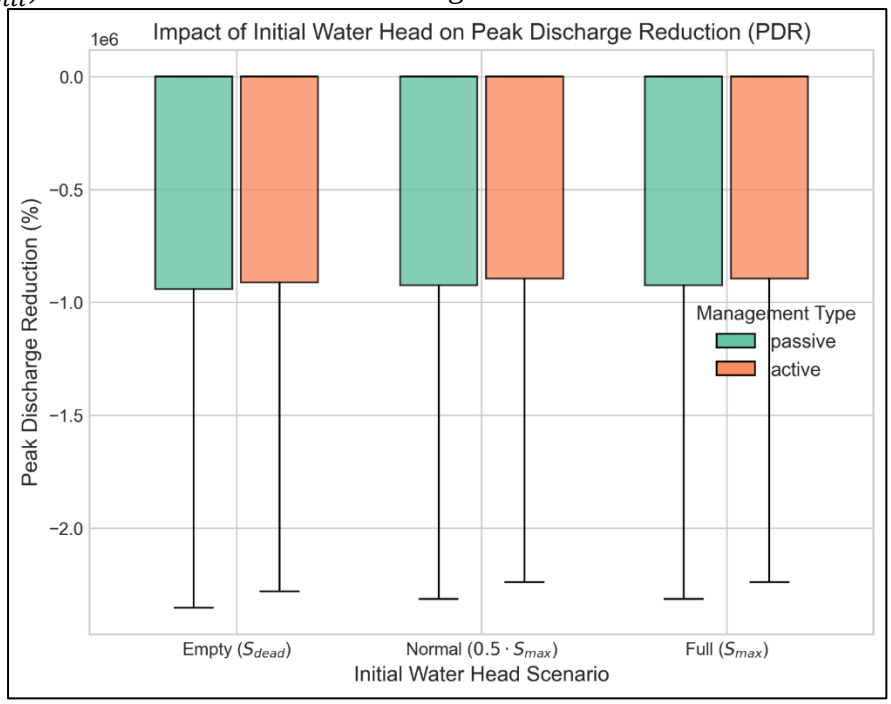

Figure 2. Impact of Initial Water Head on Peak Discharge Reduction

As presented in Table 2. Numerical constraints ensure that the initial storage capacity controls the macro-scale reduction in flood peak efficiency. Details of the distribution and comparison of peak reduction variability for each boundary condition are shown in Figure 2. *The empty reservoir scenario* ($S_{t=0} = S_{dead}$) *provides the best flood attenuation performance, achieving an average PDR of* 26.227% *and increasing to* 63.503% *in* a highly responsive catchment area. Mathematically, this condition allocates the entire initial volume of the hydrograph to meet the reservoir's dead and normal storage deficit ($\Delta S = S_{crest} - S_{dead}$). This holds the accumulated total surface runoff before the lake water level elevation (h_t) intersects the uncontrolled spillway crest (h_{crest}).

In contrast, a progressive decrease in damping capability was observed in the *Normal* scenario (average PDR = 14.341%), which culminated in a drastic decline to 6.084% under the full reservoir *scenario* ($S_{t=0} = S_{max}$). When the initial retention space has been completely exhausted, the physical flood mitigation capacity of the catchment area relies purely on the dynamic storage effect above the spillway ($h_t > h_{crest}$), which is completely controlled by the hydraulic mechanics of the spillway weir.

Temporal Shift: Peak Flow Delay (Lag Time to Peak)

Regional-scale flood wave propagation delays from upstream source cells to outlets are evaluated using the temporal shift metric (peak_delay_hours). This analysis compares the hydraulic efficiency between standard Passive Operation and

Nusantara Hasana Journal
Volume 3 No. 8 (Januari 2024), Page: 394-405
E-ISSN : 2798-1428

predictive Active Management operating with quantitative precipitation forecast (QPF) data. As summarized in Table 3.

Table 3. Comparison of Flood Peak Time Delays (Lag Time in Hours)

Initial Water Elevation Scenario	Passive Operation Scenario (Hours)	Active Management Scenario (QPF) (Hours)	Net Temporal Gain (Hours)
Empty	3.50 ± 1.2	8.20 ± 2.4	+4.70
Normal	1.80 ± 0.8	6.40 ± 1.9	+4.60
Full	0.40 ± 0.2	4.10 ± 1.5	+3.70

The capability of distributed reservoir networks to delay the propagation of flood waves was evaluated by calculating the temporal shift of hydrograph peaks under both passive and active operational strategies. The aggregated simulation results across the three antecedent storage state boundaries are illustrated in Figure 3.

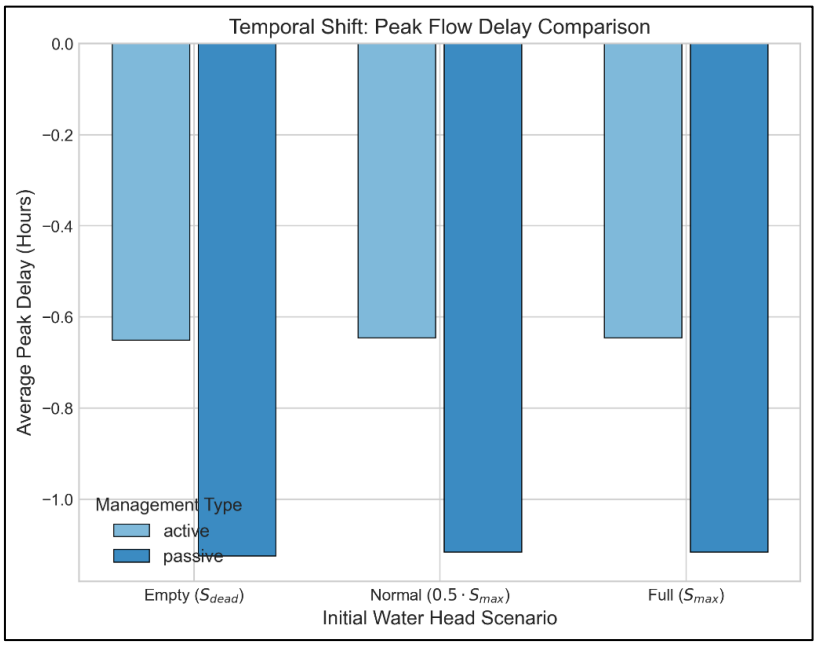

Figure 3. Temporal Shift: Peak Flow Delay Comparison

As presented in Table 3. The integration of the QPF-based Active Management scheme demonstrated a systemic advantage in delaying the arrival time of the peak discharge hydrograph across all initial water-level boundary conditions. As shown in the summary of average delay values in Figure 3, the active strategy intervention significantly extended the response time. At the critical reservoir full (*Full*) boundary condition, passive tracing produced a very small delay effect (0.40 ± 0.2 hours) because the inflow immediately triggers an uncontrolled overflow.

However, by utilizing predictive active interventions—when extreme rainfall (> 50 mm) is detected by forecast radar—the system initiates planned water releases before the storm arrives ($Q_{release}$). This predictive emptying recreates a temporary artificial storage deficit within the distributed reservoir network. The visual impact of peak flattening *and* the resulting time shift in the detailed hydrograph are illustrated in the example storm event profile in Figure 4.

Nusantara Hasana Journal
Volume 3 No. 8 (Januari 2024), Page: 394-405
E-ISSN : 2798-1428

This strategy increases the average *lag time* under full conditions to 4.10 hours, resulting in a net temporal gain of +3.70 hours. At the initial *Empty* boundary condition, active management extends the peak flood delay to an average of 8.20 hours, significantly expanding the emergency evacuation time window for downstream areas.

Spatial Distribution Dynamics of the Attenuation System

Geospatial overlay analysis, using the catchment perimeter database, reveals a strong spatial correlation between the intensity of agricultural engineering and macro-scale flood mitigation capacity.

The distributed attenuation dynamics were spatially clustered using a stratification filter based on the artificial storage depth attribute. As visualized in Figure 4, the intensive agricultural intervention group—defined by an artificial storage depth of $\geq$ 10 mm per catchment—is predominantly concentrated across the flat alluvial lowlands of the Continental United States (CONUS) that are heavily dedicated to intensive cultivation.

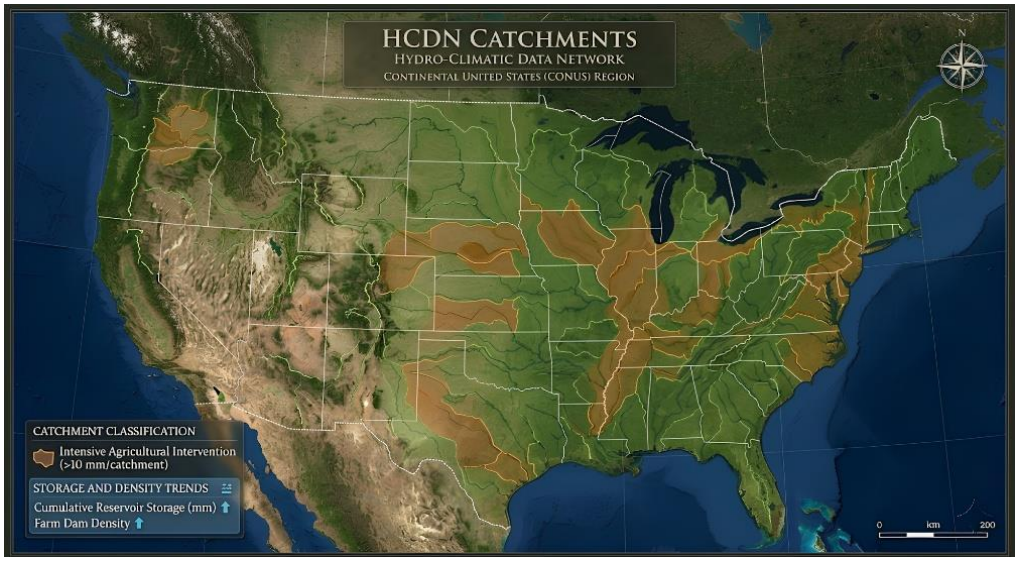

Figure 4. Spatial Geographic Distribution

Furthermore, the geographic distribution map in Figure 4 demonstrates that these heavily modified zones directly correspond to the highest peak damping efficiencies (PDR $>$ 40%). Catchments with extensive irrigation water rights and dense networks of agricultural farm dams exhibit enhanced flood retention. This spatial configuration verifies that *non-linear confluence* delays and localized flow barriers operate collectively to mitigate peak flood fluxes at a broader regional scale.

In stark contrast, upstream catchments situated along steep topographic gradients display spatial patterns with lower significance PDR values. This dichotomy reinforces the conclusion that the overall effectiveness of distributed storage networks is not merely a function of total capacity, but is highly dependent on the strategic geographic placement, topographical context, and localized geometry of reservoir storage volumes within the agricultural river network.

Nusantara Hasana Journal
Volume 3 No. 8 (Januari 2024), Page: 394-405
E-ISSN : 2798-1428

CONCLUSION

This study systematically evaluated the hydrological impacts of decentralized, distributed storage networks on peak flow attenuation and temporal delay across 47 irrigated catchments within the Continental United States (CONUS). Calibrating the distributed Large-Sample Hydrology (LSH) model using the L-BFGS-B algorithm yielded highly heterogeneous predictive reliability, with a global mean Kling-Gupta Efficiency (KGE) of 0.1657 and a peak KGE of 0.5023. The deconstruction of the KGE objective function revealed structural limitations under intensive agricultural practices, characterized by a systematic underestimation of cumulative runoff volumes ($\beta = 0.6783$) and an inflated estimate of hydrograph variability ($\alpha = 1.3360$). This underscores the critical need to incorporate high-resolution hydraulic structures and localized operational rules into large-sample conceptual routing frameworks.

The physical evaluation of flow magnitude attenuation confirmed that the antecedent water level of reservoirs serves as a primary control mechanism for peak flood mitigation. Under passive operational configurations, the empty reservoir scenario ($S_{t=0} = S_{dead}$) provided the most robust flood control, achieving a mean Peak Discharge Reduction (PDR) of 26.227% and scaling up to 63.503% in highly responsive catchments. Damping efficiency decreased markedly to 14.341% under normal conditions and further to a minimum of 6.084% under full antecedent capacity. When the physical storage deficit is completely exhausted, peak flow mitigation becomes entirely dependent on the structural surcharge dynamics over uncontrolled spillways.

In terms of temporal propagation, integrating an active management scheme utilizing Quantitative Precipitation Forecasts (QPF) proved systemically superior to conventional passive overflow routing. Active pre-storm drawdowns triggered by heavy rainfall forecasts (> 50 mm) successfully engineered artificial storage deficits across all boundary states. This proactive strategy yielded substantial net temporal gains of +3.70 to +4.70 hours compared with passive routing. Under optimal conditions, the framework extended the lag time to peak up to an average of 8.20 hours, significantly widening the critical disaster response and emergency evacuation windows for downstream communities.

Geospatial overlay analysis validated that the regional effectiveness of decentralized storage systems is heavily influenced by land-use intensity and geographic location rather than raw volumetric capacity alone. Catchments characterized by high agricultural engineering density and artificial storage depths ≥ 10 mm clustered along low-lying alluvial floodplains displayed the highest collective attenuation, with regional PDR metrics frequently exceeding 40%. Conversely, steep upstream headwater catchments demonstrated minimal attenuation capacity. Ultimately, these findings provide a quantifiable, empirical foundation for designing optimized, climate-resilient decentralized flood mitigation strategies and structural networks within heavily regulated river systems.

ACKNOWLEDGEMENTS

The author thanks the Universitas Muhammadiyah Makassar, Makassar, South Sulawesi, Indonesia, for valuable support.

Nusantara Hasana Journal
Volume 3 No. 8 (Januari 2024), Page: 394-405
E-ISSN : 2798-1428

REFERENCES

Acuña-Alonso, C., Novo, A., Rodríguez, J. L., Varandas, S., & Álvarez, X. (2022). Modelling and evaluation of land use changes through satellite images in a multifunctional catchment: Social, economic and environmental implications. *Ecological Informatics*, *71*, 101777. https://doi.org/https://doi.org/10.1016/j.ecoinf.2022.101777

Ang, R., Kinouchi, T., & Zhao, W. (2022). Evaluation of daily gridded meteorological datasets for hydrological modeling in data-sparse basins of the largest lake in Southeast Asia. *Journal of Hydrology: Regional Studies*, *42*, 101135. https://doi.org/https://doi.org/10.1016/j.ejrh.2022.101135

Armstrong, M. S., Kiem, A. S., & Vance, T. R. (2020). Comparing instrumental, palaeoclimate, and projected rainfall data: Implications for water resources management and hydrological modelling. *Journal of Hydrology: Regional Studies*, *31*, 100728. https://doi.org/https://doi.org/10.1016/j.ejrh.2020.100728

Asselman, N., de Jong, J. S., Kroekenstoel, D., & Folkertsma, S. (2022). The importance of peak attenuation for flood risk management, exemplified on the Meuse River, the Netherlands. *Water Security*, *15*, 100114. https://doi.org/https://doi.org/10.1016/j.wasec.2022.100114

Avesani, D., Galletti, A., Piccolroaz, S., Bellin, A., & Majone, B. (2021). A dual-layer MPI continuous large-scale hydrological model including Human Systems. *Environmental Modelling & Software*, *139*, 105003. https://doi.org/https://doi.org/10.1016/j.envsoft.2021.105003

Bacci, M., Dal Molin, M., Fenicia, F., Reichert, P., & Šukys, J. (2022). Application of stochastic time dependent parameters to improve the characterization of uncertainty in conceptual hydrological models. *Journal of Hydrology*, *612*, 128057. https://doi.org/https://doi.org/10.1016/j.jhydrol.2022.128057

Balkhair, K. S., Masood, A., Almazroui, M., Rahman, K. U., Bamaga, O. A., Kamis, A. S., Ahmed, I., Al-Zahrani, M. I., & Hesham, K. (2018). Groundwater share quantification through flood hydrographs simulation using two temporal rainfall distributions. *Desalination and Water Treatment*, *114*, 109–119. https://doi.org/https://doi.org/10.5004/dwt.2018.22346

Bastola, S. (2022). The regionalization of a parameter of HYMOD, a conceptual hydrological model, using data from across the globe. *HydroResearch*, *5*, 13–21. https://doi.org/https://doi.org/10.1016/j.hydres.2022.01.001

Biggs, T., Zeigler, A., & Taniguchi-Quan, K. T. (2022). Runoff and sediment loads in the Tijuana River: Dam effects, extreme events, and change during urbanization. *Journal of Hydrology: Regional Studies*, *42*, 101162. https://doi.org/https://doi.org/10.1016/j.ejrh.2022.101162

Bouizrou, I., Chahinian, N., Perrin, J.-L., Müller, R., & Rais, N. (2021). Network representation in hydrological modelling on urban catchments in data-scarce contexts: A case study on the Oued Fez catchment (Morocco). *Journal of Hydrology: Regional Studies*, *34*, 100800. https://doi.org/https://doi.org/10.1016/j.ejrh.2021.100800

Bucała-Hrabia, A., Kijowska-Strugała, M., Bryndal, T., Cebulski, J., Kiszka, K., &

Nusantara Hasana Journal
Volume 3 No. 8 (Januari 2024), Page: 394-405
E-ISSN : 2798-1428

Kroczak, R. (2020). An integrated approach for investigating geomorphic changes due to flash flooding in two small stream channels (Western Polish Carpathians). *Journal of Hydrology: Regional Studies*, *31*, 100731. https://doi.org/https://doi.org/10.1016/j.ejrh.2020.100731

Di Marco, N., Avesani, D., Righetti, M., Zaramella, M., Majone, B., & Borga, M. (2021). Reducing hydrological modelling uncertainty by using MODIS snow cover data and a topography-based distribution function snowmelt model. *Journal of Hydrology*, *599*, 126020. https://doi.org/https://doi.org/10.1016/j.jhydrol.2021.126020

Ezz, H. (2018). Integrating GIS and HEC-RAS to model Assiut plateau runoff. *The Egyptian Journal of Remote Sensing and Space Science*, *21*(3), 219–227. https://doi.org/https://doi.org/10.1016/j.ejrs.2017.11.002

Maskey, S., Kayastha, R. B., & Kayastha, R. (2020). Glacial Lakes Outburst Floods (GLOFs) modelling of Thulagi and Lower Barun Glacial Lakes of Nepalese Himalaya. *Progress in Disaster Science*, *7*, 100106. https://doi.org/https://doi.org/10.1016/j.pdisas.2020.100106

Petalas, A. L., Tsiampousi, A., Zdravkovic, L., & Potts, D. M. (2022). Numerical investigation of the performance of engineered barriers in controlling stormwater runoff. *Geomechanics for Energy and the Environment*, *32*, 100401. https://doi.org/https://doi.org/10.1016/j.gete.2022.100401

Sultan, D., Tsunekawa, A., Tsubo, M., Haregeweyn, N., Adgo, E., Meshesha, D. T., Fenta, A. A., Ebabu, K., Berihun, M. L., & Setargie, T. A. (2022). Evaluation of lag time and time of concentration estimation methods in small tropical watersheds in Ethiopia. *Journal of Hydrology: Regional Studies*, *40*, 101025. https://doi.org/https://doi.org/10.1016/j.ejrh.2022.101025

Sun, Y., Gu, X., & Xu, X. (2021). Experimental Study on Hydraulic Erosion Characteristics of Ecological Slope of Tailings Reservoir under Rainfall. *KSCE Journal of Civil Engineering*, *25*(7), 2426–2436. https://doi.org/https://doi.org/10.1007/s12205-021-0912-1

Suzuki, Y., Nakamura, K., & Hama, T. (2022). Peak discharge mitigation effects in different rainfall patterns at a paddy plot with a runoff control plate. *Journal of Hydrology: Regional Studies*, *42*, 101165. https://doi.org/https://doi.org/10.1016/j.ejrh.2022.101165

Wang, S., Peng, H., Hu, Q., & Jiang, M. (2022). Analysis of runoff generation driving factors based on hydrological model and interpretable machine learning method. *Journal of Hydrology: Regional Studies*, *42*, 101139. https://doi.org/https://doi.org/10.1016/j.ejrh.2022.101139

Yuan, S., Li, Z., Chen, L., Li, P., Zhang, Z., Zhang, J., Wang, A., & kunxia Yu. (2022). Effects of a check dam system on the runoff generation and concentration processes of a catchment on the Loess Plateau. *International Soil and Water Conservation Research*, *10*(1), 86–98. https://doi.org/https://doi.org/10.1016/j.iswcr.2021.06.007